Nanoscale

Accepted Manuscript

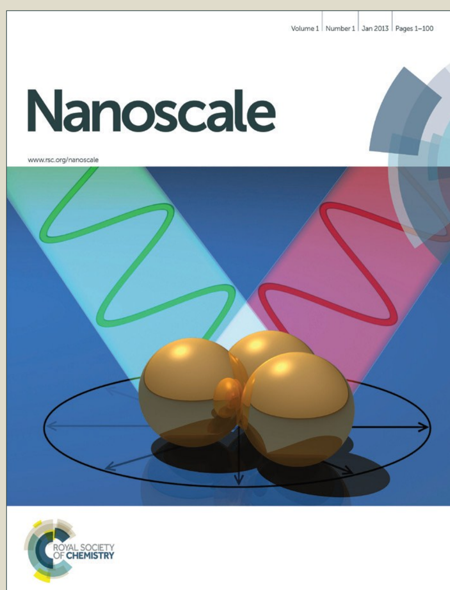

This is an *Accepted Manuscript*, which has been through the Royal Society of Chemistry peer review process and has been accepted for publication.

Accepted Manuscripts are published online shortly after acceptance, before technical editing, formatting and proof reading. Using this free service, authors can make their results available to the community, in citable form, before we publish the edited article. We will replace this *Accepted Manuscript* with the edited and formatted *Advance Article* as soon as it is available.

You can find more information about *Accepted Manuscripts* in the Information for Authors.

Please note that technical editing may introduce minor changes to the text and/or graphics, which may alter content. The journal's standard Terms & Conditions and the Ethical guidelines still apply. In no event shall the Royal Society of Chemistry be held responsible for any errors or omissions in this *Accepted Manuscript* or any consequences arising from the use of any information it contains.

ROYAL SOCIETY OF CHEMISTRY

www.rsc.org/nanoscale

Journal Name

ARTICLE TYPE

Cite this: DOI: 10.1039/xxxxxxxxxx

Fabrication of multilayered nanofluidic membranes through silicon templates

Varricchio Stefano S. G.*[a], Hibert Cyrille[b], Bertsch Arnaud[a], and Renaud Philippe[a]

Received Date
Accepted Date

DOI: 10.1039/xxxxxxxxxx

www.rsc.org/journalname

We present a new fabrication method for solid-state nanoporous membranes based on sacrificial template structures made of silicon. The process consists in creating membranes by evaporating thin-film on sacrificial templates which, after their selective removal, opens the nanopores and releases the free-standing membranes. This way is possible to define the geometry of the pore by design and to build the membrane by stacking thin-films of various materials through evaporation. Such a membrane with controlled porosity, pore geometry, thickness and nano-channel composition opens new opportunities for selective chemical functionalization, gating, electrical sensing or electrical stimulation inside the nanopore.

Nanoscale Accepted Manuscript

1 Introduction

Recent progress on nano-fabrication techniques provided unprecedented control on the properties of nanofluidic membranes which paved the way to their use in a growing list of applications. Namely, the possibility to control the span and polarity of the electric double layer (EDL) and the pore geometry extended the potential of nanoporous membranes from passive applications, such as water desalination, to active applications such as nanofluidic diodes[1,2] or transistors[3,4], which may have breakthrough applications in chemical or biological analysis, nano-medicine, filtration and energy harvesting[5–7].
Although nanofluidic impacts many fields of research the question of designing and fabricating well controlled nanodevices remains a bottleneck that impedes its development[8]. A fabrication method allowing to arbitrarily choose pores geometry, pore density, material, uniformity and that is easily integrated within common micro electromechanical systems (MEMS) technology is still missing[5,8,9].

A number of fabrication methods for solid-state nanoporous membranes were proposed which can be separated in two categories : *subtractive processes* and *additive processes*.

Subtractive processes create the nanochannel by etching it into bulk material. The geometry is defined through a mask or by serial sculpting. This usually requires less fabrication steps than additive processes and is often simpler. Track etched membranes, whose pores are defined through irradiation[10], are a good example but are limited to polymeric materials. In order to extend the choice of materials for the membranes, self-assembly properties of the anodization of aluminium were exploited to define a hard-mask for the underlying material[11]. However this approach isn't suitable if a more strict control on geometrical parameters of the nanopore is desired, since control on single-pore properties and positioning is impossible. Advances in high resolution e-beam lithography in combination with deep reactive ion etching (DRIE) allowed the fabrication of nanopores having critical dimension of 20 nm[12] and geometry controlled by design. This allowed to integrate electrodes in the nanopore even though material limitations arose from etching selectivity. Finally, probably the most flexible fabrication method in terms of geometry and materials of the membrane uses Focused Ion Beam (FIB) to drill nanopores[13,14], nevertheless due to its serial nature this approach is not appropriate to large scale production and is usually extremely time consuming.

Additive processes rely either on the control of intrinsic porosity of materials during growth/deposition (e.g. Nafion) or on template structures defining the geometry of the nanopores. Since such methods don't rely on the intrinsic properties of membrane materials, are of special interest because can be applied to a greater variety of processes. Structures made of different materials can act as template. Track-etched membranes were used as template to create nanochannels[15,16] and sacrificial layer of SiO_2 allowed to control the width of elongated nanochannels with great precision. Such membranes were shown to be integrable within drug-release implants[17,18].

[a] EPFL STI IMT LMIS4, Station 17, CH-1015 Lausanne, Switzerland. Fax: +41 21 693 59 50; Tel: +41 21 693 65 81; E-mail: stefano.varricchio@epfl.ch
[b] Center of MicroNanoTechnology, EPFL, CH-1015 Lausanne, Switzerland.

This journal is © The Royal Society of Chemistry [year]

We propose here a new additive fabrication method for nanoporous membranes based on sacrificial structures made of silicon used as template for the nanopores. The fabrication can be summarized in three parts: first, the sacrificial templates is created through e-beam lithography followed by etching; second the membrane material is deposited on and around the template; finally the selective removal of the templates reveals the pores and releases the free-standing membrane.

The rationale behind this approach, which consist of taking advantage of two well known technologies, e-beam lithography and silicon micro-machining [19], to exactly define the geometry of the nanopore, have been combined with evaporated thin-film to fabricate multi-layer and multi-materials membranes with embedded nanopores arrays. The adoption of evaporation as deposition method provide a wide choice of materials, ranging from dielectric to conductive materials and with different surface properties or chemical reactivities, uniformity of films, range of deposition (tipically 1 nm to 1000 nm), and provide the possibility to obtain multi-layers. This way functional chips with arrays of nanopores embedded in a membrane can be used to create nanofluidic devices, such as asymmetric or electrically gated nanopores. The presented process is easily integrable within a more complex process flow (e.g. for micro-fluidic channels fabrication), uses standard clean-room processes, and endows the integration of multiple membranes with different properties and geometries within the same chip. Furthermore chips with membranes of different design may be fabricated in parallel on the same wafer, which makes the process time effective compared to serial fabrication process such as FIB milling. The possibility to freely choose the pore shape plays a crucial role depending on the foreseen application. Round pores would be especially suited for electrostatic gating applications because of their higher electrode-surface-to-volume ratio with respect to other geometries. Additionally the axial symmetry of such geometry extends the influence of the EDL in the middle of the pore. Elongated pores on the other hand may be useful when a total or partial functionalization of the inner walls of the pore is needed, since the wider opening may facilitate the flow of molecules to attach. Depending on the length of the molecule the planar symmetry of the linear geometry may help to prevent steric hinderance in the middle of the channel. As proof-of-concept we fabricated chips with multilayered nanoporous membranes made of a layer of Pt between two layers of SiO_2, embedding arrays of nanopores with conical section and with different geometries.

2 Fabrication

2.1 Wafer preparation

200 nm of Si_3N_4 were grown by plasma enhanced chemical vapor deposition (PECVD) on a double side polished silicon wafer $< 100 >$ of 100 mm in diameter. The Si_3N_4 frontside was then thinned until about 60 nm remained using He/CHF_3 based DRIE, and then dipped in HF 49% for 4 minutes to remove the nitride left frontside, thus leaving a smooth and clean silicon surface for E-beam lithography. This way the backside layer is partially thinned too, but 120 nm of Si_3N_4 are left which is enough to be

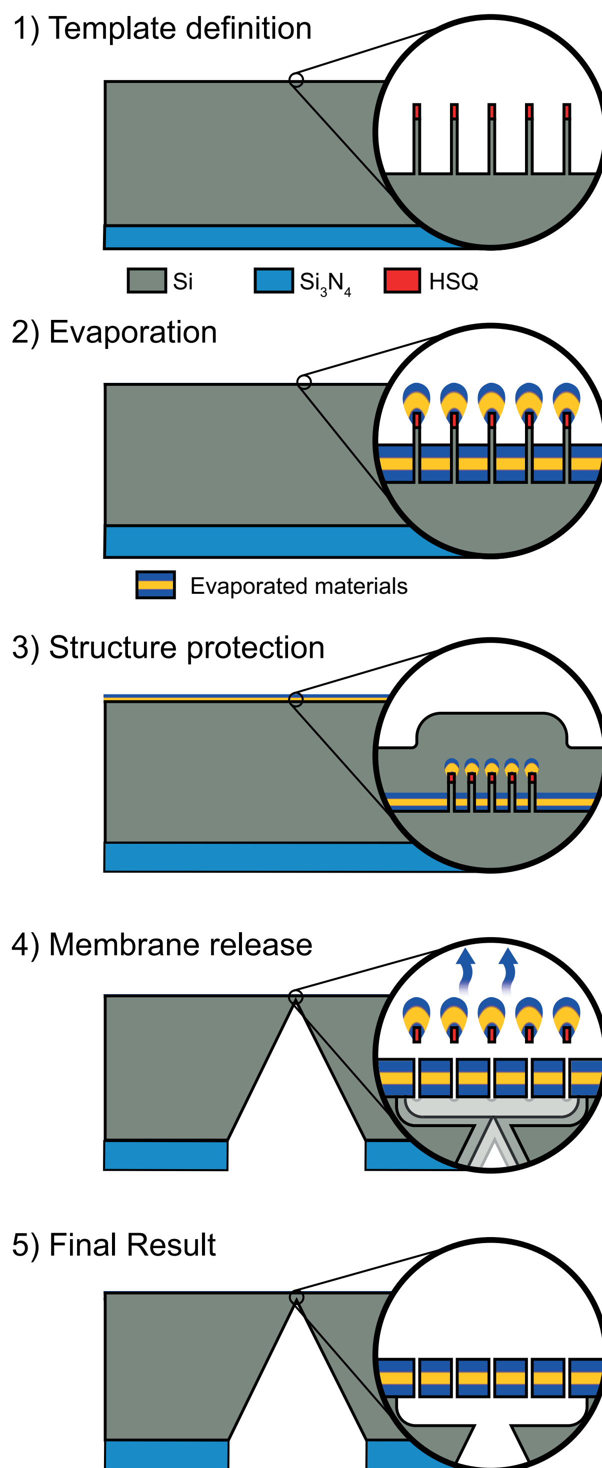

Fig. 1 Graphic representation of cross-section of the process-flow. First the sacrificial templates are made **(1)**. Then the layers composing the membrane are evaporated normal to the surface **(2)** and protected with a layer of sputtered silicon **(3)**. Finally the membrane is released through KOH etch followed by a XeF_2 pulsed etch **(4)**. The final result **(5)** is a free-standing membrane with traversing pores made of the evaporated multi-layers and with geometries defined by template.

Nanoscale Accepted Manuscript

This journal is © The Royal Society of Chemistry [year]

used as hard mask for a KOH etch step later in the process.

2.2 Sacrificial silicon structures fabrication

The nanopores geometries were defined with a frontside e-beam lithography. The wafer surface was first activated through 600 W O_2 plasma for 2 minutes to enhance e-beam resist adhesion. The wafer was then spin-coated frontside with about 140 nm of negative tone e-beam resist (hydrogen silsesquioxane (HSQ) 6% at 3000rpm). E-beam patterns were then written at dose of $8500\,\mu C\,cm^{-2}$ and developed in TMAH 25% for 2 minutes. The combination of high dose and long development time in TMAH was found to enhance both the contrast and tolerance to imprecise development time, resulting in a better reproducibility of the lithography accordingly with previously reported results[20]. Once developed the HSQ patterns were then further cross-linked through O_2 plasma, (600 W for 2 minutes), in order to increase the selectivity to the following etching step. The e-beam lithography step, due to the small surface of the membranes, takes only 90 s for the entire wafer. The sacrificial structures were finally obtained through transfer of the HSQ patterns into the wafer bulk through DRIE. More specifically a room temperature continuous anisotropic etch making use of SF_6 etchant and C_4F_8 passivator (flow rates optimized to 28 sccm and 55 sccm respectively, coil frequency 13.56 MHz, coil power 1500 W and platen power 10 W) for 4 minutes[21], which corresponds to an etch depth of about 900 nm to 940 nm (figure 1.1).

2.3 Multilayered evaporated membranes

As membrane material a Pt layer was embedded between two layers of SiO_2, with an intermediary layer of Ti to promote adhesion. We evaporated respectively: 50 nm SiO_2 + 5 nm Ti + 300 nm Pt + 5 nm Ti + 50 nm SiO_2 (figure 1.2). The layer of 5 nm of Ti was evaporated to enhance the adhesion of the SiO_2 and Pt layers. On top of that 750 nm of silicon was sputtered to momentary protect the sacrificial silicon structures during the successive backside lithography (figure 1.3). This temporary protection layer will then be removed simultaneously with the sacrificial structures in the last step of the fabrication. Platinum and SiO_2 were chosen as they are materials widely used as electrodes or insulators respectively, thus showing the potential to integrate different electrodes along the membrane. .

2.4 Membrane release

To release the membranes a combination of KOH and XeF_2 etching was used (figure 1.4). First the Si_3N_4 layer backside was structured as hard mask using standard photolithography technology ($2\,\mu m$ of AZ9260) followed by He/CHF_3 based DRIE to expose the silicon underneath. Then the wafer was etched backside with KOH (40% at 60 °C for approximately 19 hours) using a waterproof teflon chuck to protect the frontside until $5\,\mu m$ to $10\,\mu m$ of silicon were left. The wafer was then cleaved into chips with the help of a diamond pen. To finally release the freestanding membranes, the last micrometers of silicon on backside, the silicon protection layer, and the sacrificial structures were removed through XeF_2 pulsed etching in groups of 4 chips (50

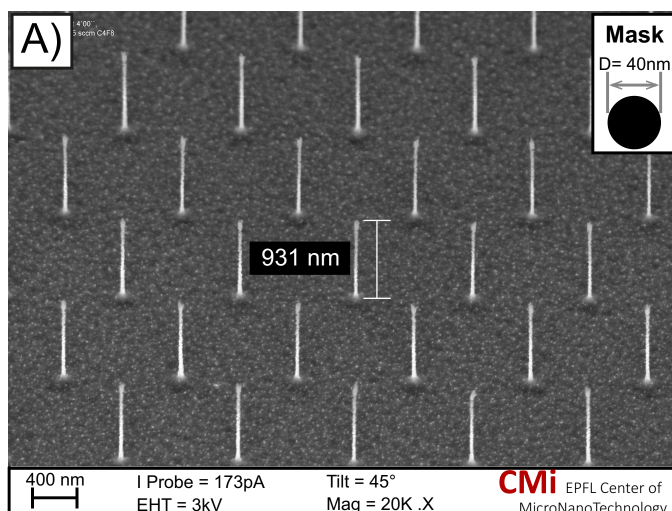

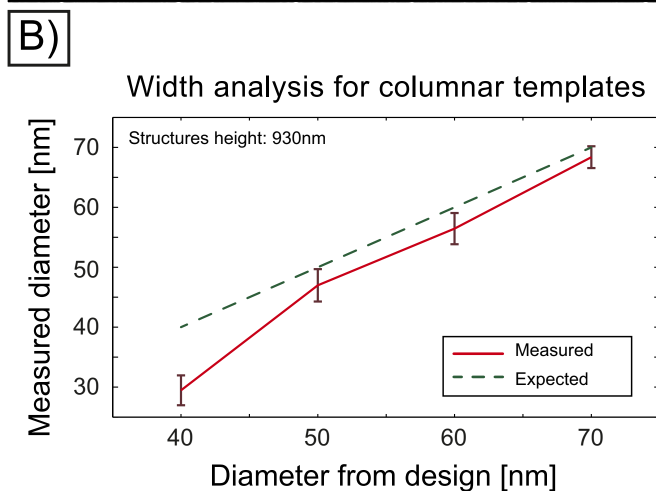

Fig. 2 SEM images showing the silicon sacrificial templates obtained after SF_6/C_4F_8 based DRIE. Figure **a)** shows an array of columns of 30 nm of diameter and 930 nm tall (aspect ratio (AR)= 31) obtained with an HSQ round mask 40 nm in diameter. Figure **b)** shows the measured diameter of columnar templates with respect to the mask design. Every measurement is obtained through image analysis of 35 structures of the same pattern and within the same wafer.

Nanoscale Accepted Manuscript

$\times$ 30 seconds at 2700 mbar). XeF_2 has the advantage to be extremely selective to silicon[22], thus removing the silicon sacrificial structures but leaving intact anything else, included the evaporated materials and thus the inner walls of the nanopores (figure 1.5). Beyond the greater selectivity XeF_2 etching in gas phase further prevents any issues related to temperature gradients, physical ion bombardment and backside pressure present with DRIE processes. XeF_2 is mainly used when high selectivity to silicon is needed, since the etchant leaves perfectly intact most of materials. This makes it highly integrable with other process-flows since non-CMOS compatible metal such as Au, Ag or Cu can be used as membrane material without contamination issues.

3 Results

3.1 Sacrificial structures

Using the fabrication process presented in the previous section, three different types of sacrificial structures with different geometries were fabricated.

Columnar structures. Round HSQ masks with diameters ranging from 10 nm to 70 nm were used to fabricate uniform arrays of columnar templates (figure 2.a shows an array of columnar templates with diameter of 40 nm). Arrays of structures up to 930 nm tall and of different diameters were obtained. To quantify their width an image analysis of scanning electron microscopy (SEM) micrographs (with magnification 50K x) was done on a pool of 35 randomly chosen structures belonging to the same array for arrays of templates with different diameters (figure 2.b). Based on those results we can observe how for 930 nm tall structures, the smallest template diameter after the etch step correspond to 40 nm. Columnar structures with smaller diameters are too fragile and collapse during the process. A reduction of diameter of about 3 nm to 5 nm due to lateral under-etch is consistently observed and becomes more pronounced for lower diameters, probably due to a local load effect, altering the ratio SF_6/C_4F_8. Using this result as a design rule, pillars with diameter of 30 nm and 930 nm tall (aspect ratio (AR) = 31) could be obtained.
The main bottleneck we observe in obtaining smaller diameter pillars consist in the AR of the HSQ mask. For a HSQ thickness of 140 nm the smallest standing structure were pillars of 30 nm in diameter. Structures with smaller footprint collapsed during the drying after development because of surface tension. Traces of collapsed HSQ masks appear after pattern transfer as small bumps of irregular shape and position as can be seen in figure 3.a).

Linear structures. Because of their shape linear structures are expected to have a higher stability than round structures, and thus to collapse less easily while drying. Fences-like structures were obtained with 1 μm long linear masks and widths ranging from 10 nm to 70 nm. With such geometry the critical dimension (CD) of the thinnest structure could be reduced to 20 nm compared to 40 nm for columnar structures (930 nm tall components), thus showing the greater stability of linear geometries with respect to round ones, as visible in figure 3.b).

Wavy structures. To further increase the stability of the templates structures, the mask design was slightly modified into a wavy line. With such a wavy design we couldn't observe any collapse of the HSQ mask while drying, even at CD=10 nm, which is a significant improvement compared to previous designs. The sacrificial structures are from now on limited by the lateral under-etch, which starts to appear in the middle of structures with CD $\leq$ 20 nm (figure 3.c). It is important to notice that, since the etching process was optimized for columnar structures, an angle of about 1° could be observed in the FIB cross-sections for linear structures, likely because a local load effect slightly alters the SF_6/C_4F_8 ratio around the structures. This may seems negligible at first sight but in the case of linear and wavy structures it results in a base consistently 20 nm wider than the tip (i.e. mask design), regardless of the size of the mask.

Etch uniformity. Characterization of the etching depth in function of the distance from the center of the wafer was carried out on four different wafers. Results shows a divergence of $\pm$5% along the radius, with a variability of less than 2% between the four different wafers.

Design This fabrication method has been used to produce 49 chips per wafer, each with an area of 9×9mm and with one membrane of $20\times20\mu$m. Each membrane is defined by an array of pores with consistent geometry (round, linear or wavy) and critical dimension (10 nm to 70 nm) such as shown in figure 2.a. The linear and wavy pores were both 1 μm long. The spacing between the pores was 1 μm, and they were disposed in an hexagonal lattice independently from the pore geometry. Therefore the membranes with round pores contained 441 pores and membranes with linear and wavy pores contained 140 pores. On the sides on the wafer test structures are present such as the ones presented in figure 3.

3.2 Evaporated thin-film

Directional deposition of thin-films through evaporation holds the promise to fabricate nanochannels made of heterogeneous materials along the pore axis using the sacrificial structures previously shown as template. As proof-of-concept we integrated a 300 nm Pt layer between two 50 nm SiO_2 layers. On top of this a protection layer of Si was sputtered to preserve the frontside during the backside processing. Figure 4.a) shows the deposition of the aforementioned layers on a linear template structure with a CD of 20 nm and 930 nm tall. The Pt and the two SiO_2 layers are well distinguishable. A fundamental aspect resulting from the choice of evaporation as deposition method is the lateral growth of the film during deposition. This results in a distinctive "cap" on top of the sacrificial structure (visible in figure 4.a which laterally grows proportionally to the thickness, thus shadowing the deposition at the base of the structure. The outcome is a conical pore with triangular section as visible on figure 4.a, which angle depends on the deposition conditions and depends from the evaporated material. In our case we measured this angle to be $28^\circ\pm2^\circ$ (Note that figure 4.a is tilted 45° and the angle is more acute than appears on the figure). One important aspect to consider is the direction-

Nanoscale Accepted Manuscript

This journal is © The Royal Society of Chemistry [year]

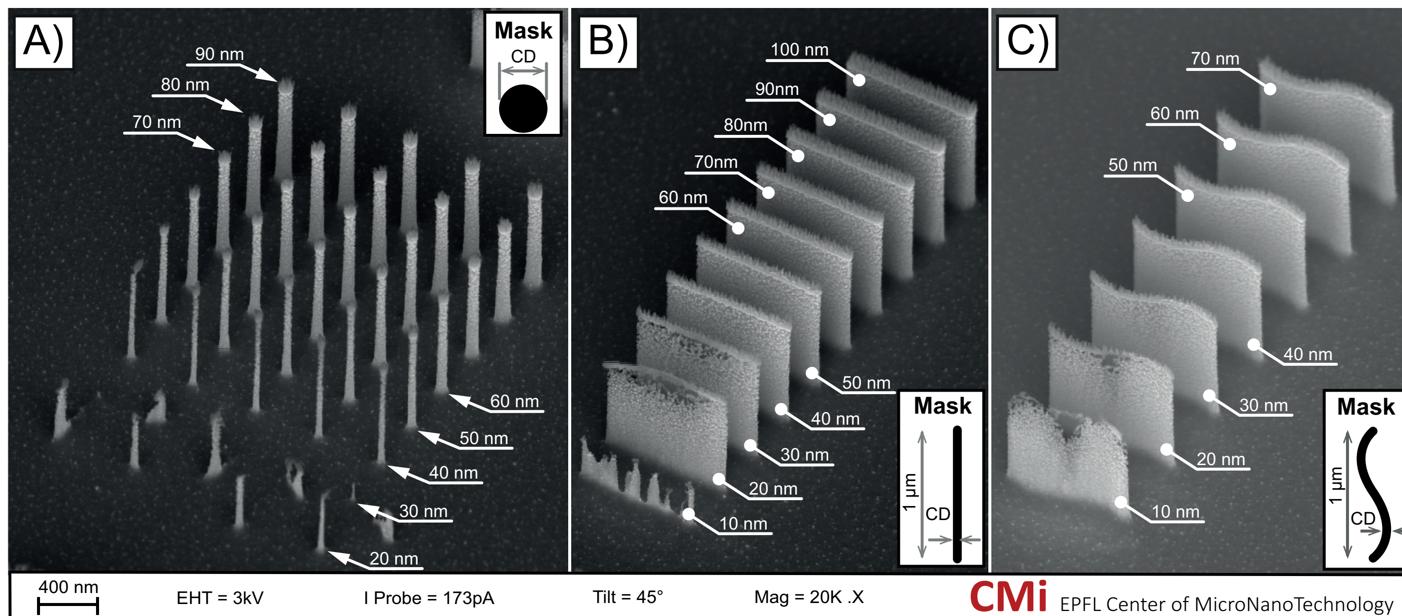

Fig. 3 SEM images showing the best achievements of the process in relation to the design of the mask for different critical dimension (CD). All the structures are 930 nm tall and have been simultaneously etched on the same wafer. The markers corresponds to the CD of the design. Figure **a)** shows an array of pillars with different diameters (CD). Smallest freestanding pillars can be seen at CD=40 nm. Smaller CD are limited by the AR of the HSQ mask. The prints of the "shadow" of collapsed masks can be guessed in correspondence of the 30 nm markers. Figure **b)** shows linear structures ranging from 10 nm to 100 nm. The smallest functional structure has a CD of 30 nm. In the structures with CD=20 nm the peel of HSQ mask start to be visible. At smaller CD the structure are limited from the AR of the HSQ mask (AR$\geq$ 14). Figure **c)** show wavy structures ranging from 10 nm to 70 nm. This particular shape prevents the HSQ mask from collapsing at low CD, reaching almost CD=10 nm.

ality of evaporation which should be as perpendicular as possible to the wafer surface. A tilted evaporation results in a deposit of material on the flank of the structure as can be seen in figure 4.a, on the left side of the template. A more pronounced tilt would deposit enough material to connect the "cap" with the membrane underneath such that during XeF_2 release it would not fall as expected but rather stay attached to the membrane, as happened in the case presented in figure 4.b. Such side deposit doesn't appear to have consequences on the nanofluidic behaviour of the membrane as long as it doesn't affect the critical dimensions of the pores.

After XeF_2 release the silicon template and the silicon protection layer visible in figure 4.a is etched away and only the evaporated material is left, resulting in a free standing membrane with porosity and pore geometry well controlled both frontside and backside as shown in figure 4.c and 4.d. Some defects (less than 1%) were observed due to the bending of some sacrificial columnar templates at CD close to the limit of stability of the structures. Those defects are only present in the membranes obtained with pillars and not in the ones from the linear and wavy templates.

In order to show the capability to stack multiple layers in the same nanopore, up to 7 layers of alternated SiO_2 and Pt layers 60 nm thick, (with 5 nm of Ti to promote adherence in between layers) have been evaporated as presented in figure 4.e.

3.3 Pore dimension

To evaluate the final dimensions of the pores, image analysis was performed on 119 pores of the membrane based on columnar templates with diameter of 40 nm (shown in figure 4.c). The result shows a CD$=$ 64 nm $\pm$ 17 nm. The final size analysis was performed on columnar structures with 40 nm of diameter since the etching process was specifically optimized to this structure.

Membranes with linear and wavy templates resulted in pores wider than expected from design (4.f) due to the wider base of the template previously mentioned and further discussed later in the document.

4 Electrical characterization

In addition to SEM inspection two different tests were conduct to assess proper definition of the membrane geometry and their integrity. First the porosity deduced through electrical conductance was compared with the value expected from design, second we quantified the current rectification effect expected due the conical shape of the nanopores. Both tests used the same experimental setup but with electrolites at different ionic strength. The setup consists in two reservoirs filled with 850 mL of KCl solution separated by the membrane to study. A voltage was then applied across the membrane with a potentiostat and the resulting current response registered. Both electrode/electrolyte interface were made by means of two Ag/AgCl electrodes fabricated by anodization of Ag wires in 0.1 M HCl solution and equilibrated

Nanoscale Accepted Manuscript

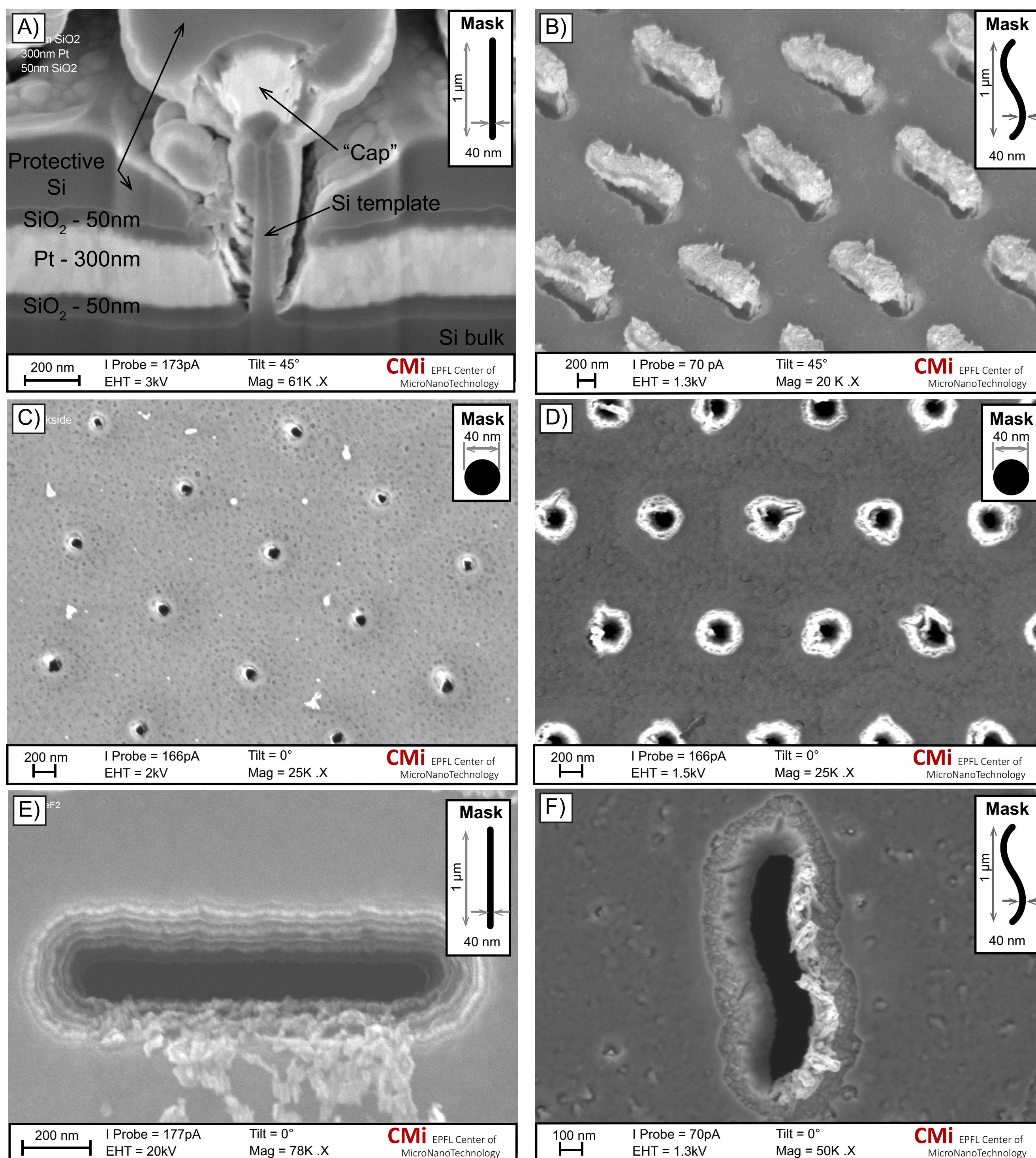

Fig. 4 SEM images showing details of the evaporation and release of the membrane. Figure **a)** shows a tilted image of FIB cross section of a linear template before XeF_2 release. The template is visible in the middle as long as the three layers of SiO_2 - Pt - SiO_2. The "cap" that creates the conical shape of the pore is visible on top of the template. Figure **b)** shows the effect of a non-perpendicular evaporation on the membrane after release. The Evaporation of material on the flanks of the template cause the caps shown in figure a)not to fall when the template is removed but to stay on the membrane. Figures **c)** and **d)** shows the backside and frontside respectively of the same membrane. The holes on the backside correspond to the small opening of the conic pore and are therefore significantly smaller than on the frontside. Figure **e)** shows a multilayered nanopore obtained by stacking 7 layers of alternated $60\,\mathrm{nm}$ of SiO_2 and $60\,\mathrm{nm}$ of Pt. A layer of $5\,\mathrm{nm}$ of Ti was used to enhance adhesion between layers. The 3 layers of Pt are well distinguishable inside the pore. Figure **f)** shows a pore obtained with a wavy template. The sub-optimal shape of the template results in a CD of the pore greater than expected from design.

Nanoscale Accepted Manuscript

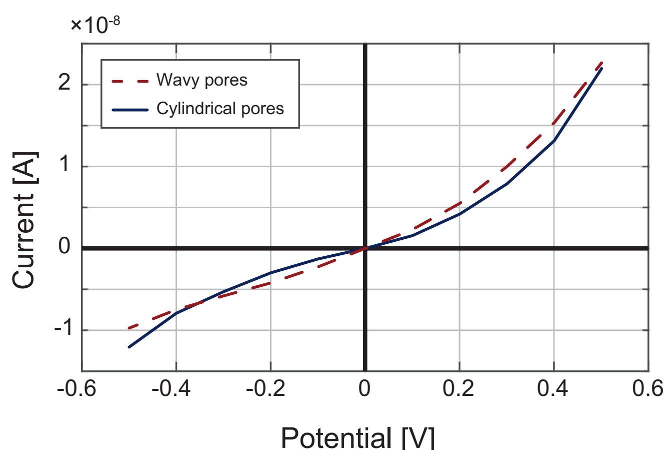

Fig. 5 Current-Voltage curves across two different membranes measured in KCl 0.1 mM electrolyte. The curves shows a slight rectification effect characteristic of pores with conical shapes, thus proving the integrity of the membrane.

overnight.
The total pore surface of the membrane was assessed by measuring the conductivity of a membrane with 441 round pores of CD= 64 nm in 1 M KCl at ±0.5 V. At such concentration the EDL effect is negligible[23] and therefore the resistivity measured is directly related to the number of pores and their surface. The measured electrical resistance of the membrane with a total pore surface of $1.89\,\mu\mathrm{m}^2$ is 5.825 MΩ ($0.906\times10^{-7}\,\mathrm{S}\mu\mathrm{m}^{-2}$). The membrane was then peeled of the chip silicon chip, leaving only the aperture made by KOH etching to connect the two reservoirs with an open a surface of $\approx 30\times30\mu$m. The resistivity measured in this case is 8.123 kΩ ($1.367\times10^{-7}\,\mathrm{S}\mu\mathrm{m}^{-2}$). Although this calculation doesn't account for different effects taking place such as the entrance resistances, it can help identify broken or defectives membranes. Here the increase in conductance when the membrane is removed is coherent with the increase of total surface, i.e. the normalized conductivities measured in both cases corresponds (0.906×10^{-7} vs. $1.367\times10^{-7}\,\mathrm{S}\mu\mathrm{m}^{-2}$) thus proving the absence of leakage and the integrity of the membrane.
The current response of two membranes was then measured. The measurement was obtained through cyclic galvanostatic chronoamperomery with steps of 0.1 V within the range −0.5 V to 0.5 V in a solution of 0.1 mM KCl. The voltage has been cycled 3 times and for each value the current has been stabilized during 180 s before measurement. The measurement is then done during 10 s with a sampling rate of 10 Hz. The results are shown in figure 5 where the ionic conductivity of two different membranes, one with round pores of 60 nm and one with wavy pores with CD of ≈ 150 nm are reported. As expected a slight rectification effect can be observed due to the conical section of the pores[24,25]. Due to the comparable overall surface of the membranes and the fact that at 0.1 mM in both membranes there is overlap of the EDL inside the pores, the behaviour of the two membranes is similar.

5 Discussion

5.1 Template shape

We identified the minimal size for the sacrificial templates 930 nm tall as 30 nm in diameter for columnar structures and 20 nm in width for linear and wavy structures. We chose this design as a trade-off between stability of the structures, structure size and structure height. The minimal size of the structure is indeed limited by two factors: the HSQ aspect ratio (limited to AR of ≈ 10) and the stability of the template. The size of the templates could therefore be reduced if a thinner layer of HSQ is used, allowing to obtain more stable masks at small sizes. A thinner mask would reduce the maximal height of the template, limited by the selectivity to HSQ of the etching process (about 10:1).
Two important parameters defining the template shape are the angle of the walls respect to the vertical and the shape of the base. Because the etching step was optimized for columnar structures (which are the most difficult to fabricate), linear and wavy templates showed walls not perfectly vertical resulting in structure with the base 40 nm consistently wider than the tip independently from their CD. This can be easily corrected by optimizing the SF_6/C_4F_8 ratio during the reactive ion etch step to the template shape. Supplementary tests reinforced this hypothesis by showing a dependence of the angle of the templates from the template density. Although the variation in the verticality of the templates is low in absolute ($\approx\pm1°$) it has a strong impact on the final shape of the pore, because it significantly increases the footprint of the structure. As visible in figure 4.a, the critical dimension of the pore depends on the width at the base of the template, resulting in an increase of the minimal pore size with respect to the design dimensions.
A secondary aspect related to the shape of the template is the angle at the junction between the template and the substrate. As visible in figure 4.a linear templates shows a rounded junction resulting in a further increase of some tenths of nanometers in the critical dimension of the nanopore. On the other hand, the opposite effect (trenching) could further weaken the stability of the template.
Since the sub-optimal etch in linear and wavy templates both over mentioned effects are clearly observable in the resulting pores such as presented in figure 4.f ($CD_{mask} = 40\,\mathrm{nm}, CD_{final} = 120\,\mathrm{nm}$)). The results were finally limited by the height of the template structure which limited the pores CD to 64 nm but we are confident that thinner membranes with pores in the order of 15 nm can be obtained with shorter templates, thinner HSQ layer and an etching step optimized to the desired template. Indeed in the case of wavy templates shown in figure 3.c the upper part of 10 nm templates already showed to not collapse at extremely small dimensions, so it's reasonable to think the limits can be pushed forward with optimization of the e-beam lithography and etching steps to a specific design.

5.2 Considerations on materials

One other fundamental characteristic of this fabrication process is the variety of materials that can be used to create the stacked membrane and the membrane thickness. Virtually any stack of

Nanoscale Accepted Manuscript

evaporable material withstanding the XeF_2 etch can be obtained, contrary to subtractive methods previously mentioned where the etching chemistry limits the process. Gold membranes of 100 nm of thickness with porosity controlled by design were also fabricated with the objective to easily functionalize the nanopores with thiols, which will be discussed in a future work. For example material-selective adhesion could be used to pattern some channel region to prevent fouling[26] or to immobilize particles of interest in the desired zones of the nanopore. Simulations have shown that the grafting of polymers inside channels could change the electric potential distribution inside the pore[27] opening new opportunities for nanofluidic developments.

Non-linear effects such as current rectification arises from the conical shape of nanopores[25]. Those properties can find application for biomolecule manipulation as well as transport control[5]. As previously shown this is due to the lateral growth of the evaporated thin-film that in our case results in a cone angle of $28^{\circ} \pm 2^{\circ}$. This peculiarity of the process depends on the evaporated material its deposition temperature and can therefore be controlled. However to our knowledge the lateral growth during evaporation strongly depend on the material and therefore design guides cannot be provided for this aspect of the fabrication.

One emblematic property of this process is the possibility to stack multiple layers of different materials to compose the pore thanks to the combination of XeF_2 and evaporation. In this case a critical aspect to consider is the stress of the thin films and their mutual adherence. This aspect is however related to all free-standing multilayered membranes and isn't a specific characteristic of this fabrication method. In our case the membrane proposed in figure figure 4.e where multiple layers of Pt and SIO_2 were stacked to compose the membrane didn't show problems of stress nor peeling after release. The variety in materials and the possibility to stack multiple layers provides unprecedented options in the choice of materials and their selective functionalization or patterning inside the nanopore, paving the way to actively gated membranes and stimulation or sensing inside the nanopore.

5.3 Significance compared to other fabrication technologies

Other methods allows to obtain multilayered and nanoporous membranes or to functionalize the nanopores surface to modify their properties.

Multimaterial membranes were used to fabricate ionic field effect transistor through substractive method[28] or used to sense DNA translocation[12]. The presented fabrication method extends the materials with which such structures can be fabricated, and in particular the materials used to embed electrodes in such devices as their electrochemical properties are of crucial importance in those applications.

Functionalization of pore surface is one other research field where this fabrication method can have an impact. Different methods able to modify the physico-chemical properties of nanopores such as atomic layered deposition (ALD) or covalent nanopore modification have been developed[29]. The presented technology will simplify and even extend the capability of such devices thanks to the wide choice of stacked evaporable material. For example partial or even heterogeneous functionalization of the same pore can be achieved through appropriate choices of membrane material and material-selective coatings.

6 Conclusions

A new method allowing the production of solid-state nanoporous membranes with controlled porosity, pore geometry, thickness and channel composition based on sacrificial template structures has been presented. This method allows to manufacture chips with multilayered membranes embedding nanoporous devices with conical pores in a wide variety of evaporable material, thus providing the possibility to control the pore material along the pore axis. The critical aspects of fabrication such as template shape and evaporation directionality have been discussed. Control on geometrical parameters of the pores such as conical section, pore shape or number of pores have been shown through electrical measurements, coherently with expectations. The unprecedented freedom in the choice of materials, pores geometries and integrability within other process-flows may endow new technological developments especially regarding chemical functionalization and active control of molecules (i.e. gating) inside the nanopores[30,31].

Acknowledgement

The authors would like to thank Niccoló Piacentini for the help during the fabrication of the devices and Thomas M. Braschler for the assistance with the measurements and the fruitful discussions. We also gratefully acknowledge the CMI (Center of Micronanotechnology) staff for their availability and valid support of clean-room processes. This work was financed by the Swiss National Science Foundation Project (FNS 200021-140493).

References

1 L.-J. Cheng and L. J. Guo, *Nano letters*, 2007, **7**, 3165–71.
2 I. Vlassiouk and Z. S. Siwy, *Nano letters*, 2007, **7**, 552–6.
3 R. Karnik, R. Fan, M. Yue, D. Li, P. Yang and A. Majumdar, *Nano letters*, 2005, **5**, 943–8.
4 S. Wu, F. Wildhaber, A. Bertsch, J. Brugger and P. Renaud, *Applied Physics Letters*, 2013, **102**, 213108.
5 C. Duan, W. Wang and Q. Xie, *Biomicrofluidics*, 2013, **7**, 026501.
6 S. Prakash, A. Piruska, E. N. Gatimu, P. W. Bohn, J. V. Sweedler and M. A. Shannon, *IEEE Sensors Journal*, 2008, **8**, 441–450.
7 R. B. Schoch, A. Bertsch and P. Renaud, *Nano Letters*, 2006, **6**, 543–547.
8 L. Bocquet and P. Tabeling, *Lab on a chip*, 2014, **14**, 3143–58.
9 M. Napoli, J. C. T. Eijkel and S. Pennathur, *Lab on a chip*, 2010, **10**, 957–985.
10 S. Chakarvarti, *Radiation Measurements*, 2009, **44**, 1085–1092.
11 S. Wu, F. Wildhaber, O. Vazquez-Mena, A. Bertsch, J. Brugger and P. Renaud, *Nanoscale*, 2012, **4**, 5718–23.
12 J. Bai, D. Wang, S.-W. Nam, H. Peng, R. Bruce, L. Gignac, M. Brink, E. Kratschmer, S. Rossnagel, P. Waggoner, K. Reuter,

Nanoscale Accepted Manuscript

This journal is © The Royal Society of Chemistry [year]

C. Wang, Y. Astier, V. Balagurusamy, B. Luan, Y. Kwark, E. Joseph, M. Guillorn, S. Polonsky, A. Royyuru, S. Papa Rao and G. Stolovitzky, *Nanoscale*, 2014, **6**, 8900–6.

13 J. Li, D. Stein, C. McMullan, D. Branton, M. J. Aziz and J. Golovchenko, *Nature*, 2001, **412**, 166–169.

14 Y. Xu and N. Matsumoto, *RSC Advances*, 2015, **5**, 50638–50643.

15 S. Chakarvarti and J. Vetter, *Radiation Measurements*, 1998, **29**, 149–159.

16 N. Sobel, C. Hess, M. Lukas, A. Spende, B. Stühn, M. E. Toimil-Molares and C. Trautmann, *Beilstein Journal of Nanotechnology*, 2015, **6**, 472–479.

17 F. Martin, R. Walczak, A. Boiarski, M. Cohen, T. West, C. Cosentino, J. Shapiro and M. Ferrari, *Journal of Controlled Release*, 2005, **102**, 123–133.

18 W.-H. Chu, R. Chin, T. Huen and M. Ferrari, *Journal of Microelectromechanical Systems*, 1999, **8**, 34–42.

19 H. Gardeniers and A. Van den Berg, *International Journal of Environmental Analytical Chemistry*, 2004, **84**, 809–819.

20 G. Singh, P. Stenberg, P. Vahima, M. Kuittinen, R. P. Yadav and V. Janyani, Proceedings of SPIE, 2011, p. 792715.

21 C. Hibert, J. O'Brien, B. McCarthy, A. M. Kelleher, B. O'Neill and P. J. Hughes, MNE 2005: Proceedings of the 31st International Conference on Micro and Nano Engineering, Wien, 2005.

22 K. R. Williams, K. Gupta and M. Wasilik, *Journal of Microelectromechanical Systems*, 2003, **12**, 761–778.

23 W. Sparreboom, A. Van den Berg and J. C. T. Eijkel, *Nature nanotechnology*, 2009, **4**, 713–20.

24 J. Cervera, B. Schiedt and P. Ramírez, *Europhysics Letters (EPL)*, 2005, **71**, 35–41.

25 J. Cervera, B. Schiedt, R. Neumann, S. Mafé and P. Ramírez, *The Journal of chemical physics*, 2006, **124**, 104706.

26 M. Zhang, T. A. Desai and M. Ferrari, *Biomaterials*, 1998, **19**, 953–960.

27 O. Peleg, M. Tagliazucchi, M. KroÌĹger, Y. Rabin and I. Szleifer, *ACS nano*, 2011, **5**, 4737–4747.

28 S.-W. Nam, M. J. Rooks, K.-B. Kim and S. M. Rossnagel, *Nano Letters*, 2009, **9**, 2044–2048.

29 J. Kudr, S. Skalickova, L. Nejdl, A. Moulick, B. Ruttkay-Nedecky, V. Adam and R. Kizek, *Electrophoresis*, 2015, **36**, 2367–2379.

30 I. Y. Wong, B. D. Almquist and N. A. Melosh, *Materials Today*, 2010, **13**, 14–22.

31 L. J. Steinbock and a. Radenovic, *Nanotechnology*, 2015, **26**, 074003.

Nanoscale Accepted Manuscript